Biomedical Optics EXPRESS

Gold nanoparticle targeted photoacoustic cavitation for potential deep tissue imaging and therapy

Hengyi Ju,[1] Ronald A. Roy,[2] and Todd W. Murray[1,*]

[1]*Department of Mechanical Engineering, University of Colorado at Boulder, 427 UCB Engineering Center, Boulder, CO 80309, USA*

[2]*Department of Mechanical Engineering, Boston University, 110 Cummington Street, Boston, MA 02215, USA*

**todd.murray@colorado.edu*

Abstract: The laser generation of vapor bubbles around plasmonic nanoparticles can be enhanced through the application of an ultrasound field; a technique referred to as photoacoustic cavitation. The combination of light and ultrasound allows for bubble formation at lower laser fluence and peak negative ultrasound pressure than can be achieved using either modality alone. The growth and collapse of these bubbles leads to local mechanical disruption and acoustic emission, and can potentially be used to induce and monitor tissue therapy. Photoacoustic cavitation is investigated for a broad range of ultrasound pressures and nanoparticle concentrations for gold nanorods and nanospheres. The cavitation threshold fluences for both nanoparticle types are found to drastically reduce in the presence of an ultrasound field. The results indicate that photoacoustic cavitation can potentially be produced at depth in biological tissue without exceeding the safety limits for ultrasound or laser radiation at the tissue surface.

OCIS codes: (170.0170) Medical optics and biotechnology; (170.5120) Photoacoustic imaging; (170.5180) Photodynamic therapy.

References and links

1. S. Link and M. A. El-Sayed, "Optical properties and ultrafast dynamics of metallic nanocrystals," Annu. Rev. Phys. Chem. **54**(1), 331–366 (2003).
2. X. Yang, E. W. Stein, S. Ashkenazi, and L. V. Wang, "Nanoparticles for photoacoustic imaging," Wiley Interdiscip Rev Nanomed Nanobiotechnol **1**(4), 360–368 (2009).
3. S. Y. Emelianov, P.-C. Li, and M. O'Donnell, "Photoacoustics for molecular imaging and therapy," Phys. Today **62**(5), 34–39 (2009).
4. T. B. Huff, L. Tong, Y. Zhao, M. N. Hansen, J.-X. Cheng, and A. Wei, "Hyperthermic effects of gold nanorods on tumor cells," Nanomedicine (Lond) **2**(1), 125–132 (2007).
5. X. Huang, P. K. Jain, I. H. El-Sayed, and M. A. El-Sayed, "Plasmonic photothermal therapy (PPTT) using gold nanoparticles," Lasers Med. Sci. **23**(3), 217–228 (2008).
6. V. P. Zharov, V. Galitovsky, and M. Viegas, "Photothermal detection of local thermal effects during selective nanophotothermolysis," Appl. Phys. Lett. **83**(24), 4897–4899 (2003).
7. D. O. Lapotko, E. Lukianova, and A. A. Oraevsky, "Selective laser nano-thermolysis of human leukemia cells with microbubbles generated around clusters of gold nanoparticles," Lasers Surg. Med. **38**(6), 631–642 (2006).
8. V. K. Pustovalov, A. S. Smetannikov, and V. P. Zharov, "Photothermal and accompanied phenomena of selective nanophotothermolysis with gold nanoparticles and laser pulses," Laser Phys. Lett. **5**(11), 775–792 (2008).
9. X. Huang, B. Kang, W. Qian, M. A. Mackey, P.-C. Chen, A. K. Oyelere, I. H. El-Sayed, and M. A. El-Sayed, "Comparative study of photothermolysis of cancer cells with nuclear-targeted or cytoplasm-targeted gold nanospheres: continuous wave or pulsed lasers," J. Biomed. Opt. **15**(5), 058002 (2010).
10. R. R. Anderson and J. A. Parrish, "Selective photothermolysis: precise microsurgery by selective absorption of pulsed radiation," Science **220**(4596), 524–527 (1983).
11. V. P. Zharov, R. R. Letfullin, and E. N. Galitovskaya, "Microbubbles-overlapping mode for laser killing of cancer cells with absorbing nanoparticle clusters," J. Phys. D Appl. Phys. **38**(15), 2571–2581 (2005).

#177949 - $15.00 USD Received 12 Oct 2012; revised 30 Nov 2012; accepted 7 Dec 2012; published 11 Dec 2012

12. D. Lapotko, E. Lukianova, A. Shnip, G. Zheltov, M. Potapnev, V. Savitsky, O. Klimovich, and A. Oraevsky, "Laser activated nanothermolysis of leukemia cells monitored by photothermal microscopy," Proc. SPIE **5697**, 82–89 (2005).
13. L. Tong, Y. Zhao, T. B. Huff, M. N. Hansen, A. Wei, and J.-X. Cheng, "Gold nanorods mediate tumor cell death by compromising membrane integrity," Adv. Mater. (Deerfield Beach Fla.) **19**(20), 3136–3141 (2007).
14. C. Ungureanu, R. Kroes, W. Petersen, T. A. M. Groothuis, F. Ungureanu, H. Janssen, F. W. B. van Leeuwen, R. P. H. Kooyman, S. Manohar, and T. G. van Leeuwen, "Light interactions with gold nanorods and cells: implications for photothermal nanotherapeutics," Nano Lett. **11**(5), 1887–1894 (2011).
15. E. Y. Lukianova-Hleb, C. Santiago, D. S. Wagner, J. H. Hafner, and D. O. Lapotko, "Generation and detection of plasmonic nanobubbles in zebrafish," Nanotechnology **21**(22), 225102 (2010).
16. E. Y. Lukianova-Hleb, I. I. Koneva, A. O. Oginsky, S. La Francesca, and D. O. Lapotko, "Selective and self-guided micro-ablation of tissue with plasmonic nanobubbles," J. Surg. Res. **166**(1), e3–e13 (2011).
17. S. Peeters, M. Kitz, S. Preisser, A. Wetterwald, B. Rothen-Rutishauser, G. N. Thalmann, C. Brandenberger, A. Bailey, and M. Frenz, "Mechanisms of nanoparticle-mediated photomechanical cell damage," Biomed. Opt. Express **3**(3), 435–446 (2012).
18. K. Wilson, K. Homan, and S. Emelianov, "Biomedical photoacoustics beyond thermal expansion using triggered nanodroplet vaporization for contrast-enhanced imaging," Nat Commun **3**, 618 (2012).
19. L. J. E. Anderson, E. Hansen, E. Y. Lukianova-Hleb, J. H. Hafner, and D. O. Lapotko, "Optically guided controlled release from liposomes with tunable plasmonic nanobubbles," J. Control. Release **144**(2), 151–158 (2010).
20. V. Kotaidis, C. Dahmen, G. von Plessen, F. Springer, and A. Plech, "Excitation of nanoscale vapor bubbles at the surface of gold nanoparticles in water," J. Chem. Phys. **124**(18), 184702 (2006).
21. D. Lapotko, "Optical excitation and detection of vapor bubbles around plasmonic nanoparticles," Opt. Express **17**(4), 2538–2556 (2009).
22. J.-W. Kim, E. I. Galanzha, E. V. Shashkov, H.-M. Moon, and V. P. Zharov, "Golden carbon nanotubes as multimodal photoacoustic and photothermal high-contrast molecular agents," Nat. Nanotechnol. **4**(10), 688–694 (2009).
23. M. Kitz, S. Preisser, A. Wetterwald, M. Jaeger, G. N. Thalmann, and M. Frenz, "Vapor bubble generation around gold nano-particles and its application to damaging of cells," Biomed. Opt. Express **2**(2), 291–304 (2011).
24. D. Lapotko, E. Lukianova, M. Potapnev, O. Aleinikova, and A. Oraevsky, "Method of laser activated nano-thermolysis for elimination of tumor cells," Cancer Lett. **239**(1), 36–45 (2006).
25. V. P. Zharov, K. E. Mercer, E. N. Galitovskaya, and M. S. Smeltzer, "Photothermal nanotherapeutics and nanodiagnostics for selective killing of bacteria targeted with gold nanoparticles," Biophys. J. **90**(2), 619–627 (2006).
26. E. Y. Lukianova-Hleb, A. O. Oginsky, A. P. Samaniego, D. L. Shenefelt, D. S. Wagner, J. H. Hafner, M. C. Farach-Carson, and D. O. Lapotko, "Tunable plasmonic nanoprobes for theranostics of prostate cancer," Theranostics **1**, 3–17 (2011).
27. G. Akchurin, B. Khlebtsov, G. Akchurin, V. Tuchin, V. Zharov, and N. Khlebtsov, "Gold nanoshell photomodification under a single-nanosecond laser pulse accompanied by color-shifting and bubble formation phenomena," Nanotechnology **19**(1), 015701 (2008).
28. E. Lukianova-Hleb, Y. Hu, L. Latterini, L. Tarpani, S. Lee, R. A. Drezek, J. H. Hafner, and D. O. Lapotko, "Plasmonic nanobubbles as transient vapor nanobubbles generated around plasmonic nanoparticles," ACS Nano **4**(4), 2109–2123 (2010).
29. F. Rudnitzki, M. Bever, R. Rahmanzadeh, K. Brieger, E. Endl, J. Groll, and G. Hüttmann, "Bleaching of plasmon-resonance absorption of gold nanorods decreases efficiency of cell destruction," J. Biomed. Opt. **17**(5), 058003 (2012).
30. V. P. Zharov, E. N. Galitovskaya, C. Johnson, and T. Kelly, "Synergistic enhancement of selective nanophotothermolysis with gold nanoclusters: potential for cancer therapy," Lasers Surg. Med. **37**(3), 219–226 (2005).
31. D. Lapotko, E. Lukianova-Hleb, S. Zhdanok, B. Rostro, R. Simonette, J. Hafner, M. Konopleva, M. Andreeff, A. Conjusteau, and A. Oraevsky, "Photothermolysis by laser-induced microbubbles generated around gold nanorod clusters selectively formed in leukemia cells," Proc. SPIE **6856**, 68560K, 68560K-9 (2008).
32. C. H. Farny, T. Wu, R. G. Holt, T. W. Murray, and R. A. Roy, "Nucleating cavitation from laser-illuminated nanoparticles," Acoust. Res. Lett. Online **6**(3), 138–143 (2005).
33. J. R. McLaughlan, R. A. Roy, H. Ju, and T. W. Murray, "Ultrasonic enhancement of photoacoustic emissions by nanoparticle-targeted cavitation," Opt. Lett. **35**(13), 2127–2129 (2010).
34. B. Krasovitski, H. Kislev, and E. Kimmel, "Modeling photothermal and acoustical induced microbubble generation and growth," Ultrasonics **47**(1-4), 90–101 (2007).
35. T. Wu, C. H. Farny, R. A. Roy, and R. G. Holt, "Modeling cavitation nucleation from laser-illuminated nanoparticles subjected to acoustic stress," J. Acoust. Soc. Am. **130**(5), 3252–3263 (2011).
36. H. G. Flynn and C. C. Church, "Erratum: transient pulsations of small gas bubbles in water [J. Acoust. Soc. Am. 84, 985-998 (1988)]," J. Acoust. Soc. Am. **84**(5), 1863–1876 (1988).
37. T. G. Leighton, *The Acoustic Bubble* (Academic, London, 1994).
38. H. J. Maris, "Introduction to the physics of nucleation," C. R. Phys. **7**(9-10), 946–958 (2006).

#177949 - $15.00 USD Received 12 Oct 2012; revised 30 Nov 2012; accepted 7 Dec 2012; published 11 Dec 2012

39. T. R. Nelson, J. B. Fowlkes, J. S. Abramowicz, and C. C. Church, "Ultrasound biosafety considerations for the practicing sonographer and sonologist," J. Ultrasound Med. **28**(2), 139–150 (2009).
40. American National Standards Institute, "American National Standard for Safe Use of Lasers," ANSI Z136.1–2000 (Laser Institute of America, 2000).
41. A. Pifferi, J. Swartling, E. Chikoidze, A. Torricelli, P. Taroni, A. Bassi, S. Andersson-Engels, and R. Cubeddu, "Spectroscopic time-resolved diffuse reflectance and transmittance measurements of the female breast at different interfiber distances," J. Biomed. Opt. **9**(6), 1143–1151 (2004).

1. Introduction

Plasmonic nanoparticles are efficient at converting light into heat when excited at the plasmon resonance wavelength, where the optical absorption efficiency is maximized [1]. A variety of medical applications, including both imaging and therapy, have been described which use nanoparticles as nano-heat sources within tissue [2–9]. In terms of imaging, strong photothermal conversion efficiency translates into efficient generation of acoustic waves through the thermoelastic mechanism, and there has been widespread interest in using plasmonic nanoparticles as contrast agents for photoacoustic imaging [2,3]. For therapeutic applications, nanoparticle targeted regions of tissue can be selectively heated using continuous wave laser sources, producing hyperthermia and inducing cell death in the targeted region [4,5]. Alternatively, pulsed lasers can be used to illuminate nanoparticle targeted regions, with the potential advantage that due to the short illumination time the diffusion of heat is limited, thereby localizing the therapeutic effect and limiting collateral tissue damage [6–10]. There is growing evidence that the mechanism of cell death in the pulsed laser case is not thermal in nature, but rather mechanical and associated with cavitation, i.e. the growth and collapse of nano- and micro-bubbles around illuminated nanoparticles [11–14].

Cavitation around laser heated nanoparticles produces a strong and localized mechanical disruption which has been shown to be effective in producing localized cell death in nanoparticle targeted cells [15–17]. Bubble formation can also produce an enhanced photoacoustic response which can be used to monitor a therapeutic process [18]. In addition, light controlled release of chemicals from nanoparticle-loaded liposomes using nanobubbles has been demonstrated [19]. One of the principle limitations in applications involving nanoparticle targeted photonic cavitation is the high optical fluence required to nucleate and grow the bubble. Bubble formation begins when the superheated liquid surrounding the nanoparticle approaches the spinodal temperature of water (~550 K), and additional optical energy is required for subsequent bubble growth [20]. The cavitation threshold fluence depends on the nanoparticle size and type, as well as the illumination wavelength and pulse width [21,22]. For gold nanospheres illuminated at a wavelength of 532 nm with a Q-switched laser pulse, cavitation threshold fluences reported in the literature vary in the range from 46 to 2000 mJ/cm^2 [11,12,23–26], well above the maximum permissible exposure for tissue. The threshold fluences for gold nanorods (~32 mJ/cm^2) [22,26] and nanoshells (4-42 mJ/cm^2) [22,27,28] are somewhat lower and these particles have the additional advantage that they can operate in the near-IR region of the spectrum. They are, however, less stable under high optical fluence, and can exhibit permanent bleaching associated with melting induced shape change and fragmentation [29].

The cavitation threshold fluence can be reduced through nanoparticle aggregation [7,11,12,17,30,31]. Closely spaced clumps of nanoparticles exhibit a lower threshold due to overlapping thermal fields and, perhaps, plasmonic coupling between nanoparticles producing enhanced optical absorption at a particular wavelength. Nanoparticle coupling can potentially allow for improved specificity in nanobubble formation, where bubble formation is only achieved in cells with strong accumulation of nanoparticles. The threshold fluence, however, depends strongly on the particular nanoparticle distribution. A second means to decrease the threshold fluence is to reduce the local pressure at the nanoparticle position during the time of illumination using an applied ultrasound field; a process referred to as photoacoustic cavitation [32,33]. It has been shown that nanospheres subjected to negative pressure, such as

#177949 - $15.00 USD Received 12 Oct 2012; revised 30 Nov 2012; accepted 7 Dec 2012; published 11 Dec 2012

encountered during the rarefaction phase of the applied ultrasound field, have a drastically reduced cavitation threshold fluence. Furthermore, accelerated bubble growth under acoustic tension results in a substantial increase in the maximum bubble size and subsequent collapse energy, thereby enhancing both mechanical bioeffects and the amplitude of acoustic emissions.

Nanoparticle targeted photoacoustic cavitation has been reported using gold nanospheres over a limited applied ultrasound pressure range [32,33]. Further studies are required to evaluate the suitability of photoacoustic cavitation for potential *in-vivo* therapeutic applications. In this work, photoacoustic cavitation is investigated for a broad range of ultrasound pressures and nanoparticle concentrations for both gold nanospheres illuminated at 532 nm and gold nanorods illuminated at 724 nm. In the case of nanorods, the fluence at which shape change (permanent bleaching) is initiated is identified and compared to the threshold fluence for cavitation. Finally, the potential for achieving nanoparticle targeted cavitation at depth within biological tissue is discussed.

2. Experimental methods

A schematic of the experimental set-up is shown in Fig. 1. Nanoparticles in water suspension were diluted to the desired concentration using ultrapure water (Sigma-Aldrich W4502) and placed in an optically transparent polymer (low-density polyethylene) bag. This bag was then submerged in degassed water in the test tank. Two types of nanoparticles were investigated: 82 nm diameter gold nanospheres (Nanopartz 13-80) with an absorption peak at 542 nm and 25 nm × 81 nm gold nanorods (Nanopartz 30-25-750) with a longitudinal absorption peak at 724 nm.

A high intensity focused ultrasound (HIFU) transducer (Sonic Concepts H101) was used to apply the external ultrasound field. The HIFU transducer had a center frequency of 1.1 MHz, a diameter of 64.0 mm, a focal length of 63.2 mm, and a full-width-half-max (FWHM) focal diameter of 2.1 mm. The transducer was calibrated at 1.0 MHz using a 0.2 mm needle hydrophone (Precision Acoustics). A two-cycle 1.0 MHz tone burst generated by a function generator (Stanford Research Systems DS345) and sent through a power amplifier (ENI 350L) and impedance matching box was used to drive the transducer. Broadband noise characteristic of inertial cavitation activity in the nanoparticle suspension was detected using a passive cavitation detector (PCD) consisting of a 5.0 MHz focused ultrasound transducer (Olympus NDT A309S) with a diameter of 12.7 mm and a focal length of 50.8 mm. The transducer output was sent through a 40 dB preamplifier (Olympus NDT Preamp 5678) and on to a digital oscilloscope (Lecroy LC684DM). This transducer was oriented confocal to the

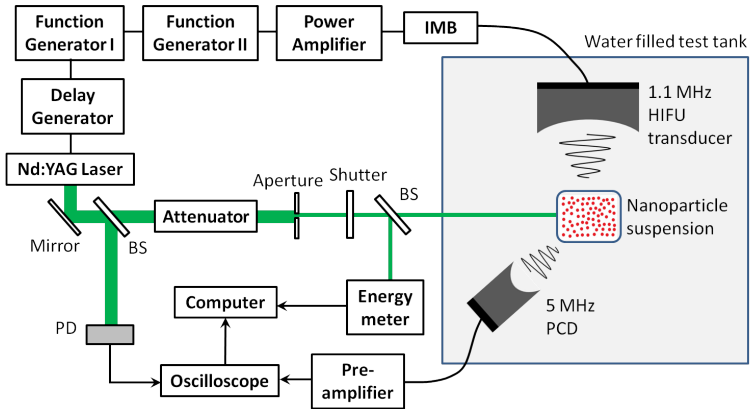

Fig. 1. Schematic of the experimental setup. Abbreviations: IMB, impedance matching box; BS, beam splitter; PD, photodetector; HIFU, high intensity focused ultrasound; PCD, passive cavitation detector.

#177949 - $15.00 USD Received 12 Oct 2012; revised 30 Nov 2012; accepted 7 Dec 2012; published 11 Dec 2012

HIFU transducer and at an angle of approximately 45 degrees relative to the HIFU axis, as shown in Fig. 1.

The nanoparticles were illuminated using a Q-switched laser source at a wavelength of either 532 nm (nanospheres) or 724 nm (nanorods) and a pulse width of 7 ns. In the case of 532 nm illumination, the output of the laser (Continuum Surelite I-20) was frequency doubled and directed through an aperture to the test tank. At the position of the nanoparticle suspension, the beam had a top-hat profile with a diameter of 1.23 mm. For 724 nm illumination, the beam was sent to an optical parametric oscillator (OPO; Continuum Surelite OPO Plus) tuned to the appropriate wavelength. The beam was then sent through a microlens array (Thorlabs MLA150-7AR) which served as a homogenizer and on to the sample. The beam profile at the sample, determined through a knife edge measurement, was nearly Gaussian with a diameter ($1/e$) of 5.40 mm. The laser energy was controlled by a variable attenuator (Newport NRC 935-10) and monitored via an energy meter (Thorlabs PM100 with sensor ES111C).

The optical axis was aligned perpendicular to the HIFU acoustic axis and in the HIFU focal plane, creating an overlap or interaction region between the two fields. The laser was then timed to fire when this interaction region was subjected to negative pressure from the second cycle of the two-cycle HIFU tone burst. A fixed delay between the ultrasound and laser pulse was obtained using a second function generator (Stanford Research Systems DS345) which sent a square pulse serving as a trigger for both the ultrasound and the laser flashlamps. The leading edge of this pulse of length τ_1 triggered the flashlamps while the trailing edge triggered the ultrasound pulse. A digital delay generator (Stanford Research Systems DG535) was then used to open the laser Q-switch and illuminate the sample at a delay τ_2 after the flashlamps were fired. The net result was that the laser was fired at a delay time of $\tau_2 - \tau_1$ after the ultrasound, with a timing jitter of less than 2.0 ns. In order to set the correct time delay, both the HIFU and laser fields were aligned to a small spherical target. The scattered HIFU pulse and the photoacoustic signal generated by the target were detected using the PCD. As the photoacoustic signal was generated at the time of laser illumination, it provided a reference point that was compared to the scattered HIFU field to determine the phase of the HIFU tone burst at the target at the time of illumination. The time delay was then adjusted such that the target was under peak negative pressure during the time of illumination. The total delay time was approximately 42.1 μs.

Under a given local pressure, pulsed laser irradiated nanoparticles undergo heating and subsequent vaporization of a thin layer of surrounding fluid, producing a vapor cavity [34,35]. At a critical size, this vapor cavity will rapidly expand and collapse through a process known as inertial cavitation [36,37]. The presence of an inertial cavitation event within the light-ultrasound region was determined based on the transient acoustic emission signal detected from this region. Cavitation probability was used to describe the likelihood of observing an inertial cavitation event under a given laser fluence, peak negative ultrasound pressure, and nanoparticle concentration. In the absence of such an event, the photoacoustic signal from the interaction region was well below the noise level of the system due to the fact that the nanoparticle concentrations used were quite low and the nanoparticles were not geometrically confined to generate an acoustic response within the bandwidth of the 5 MHz PCD. Moreover, the acoustic scattering cross section of the particles alone was not sufficient to scatter appreciable energy from the incident HIFU pulse (and its harmonics) into the PCD aperture. Inertial cavitation, on the other hand, produced a clear, transient signal that was well above the noise level. An inertial cavitation event was defined as one in which the acoustic signal within a 2.0 μs time window around the expected arrival time exceeded a threshold voltage set at approximately twice the peak noise voltage. The cavitation probability is simply defined as the number of inertial cavitation events detected divided by the total number of laser shots.

#177949 - $15.00 USD Received 12 Oct 2012; revised 30 Nov 2012; accepted 7 Dec 2012; published 11 Dec 2012

3. Results and discussion

In order to determine the effects of optical fluence and ultrasound pressure on the photoacoustic cavitation threshold of the 82-nm diameter gold nanospheres, the nanoparticle suspension was first diluted to a concentration of 2.2×10^8 nanoparticles/ml and placed in the test tank. Typical acoustic signals observed in the presence and absence of inertial cavitation are shown in Fig. 2(a). The waveforms were taken at a peak negative HIFU pressure of 1.5 MPa and a laser fluence of 4.8 mJ/cm^2. In the presence of inertial cavitation, there is a strong acoustic arrival at approximately 35 μs after the laser is fired associated with bubble collapse. In addition, arrivals associated with rebound of the bubbles and subsequent collapses are often observed at later times, particularly under high ultrasound pressure amplitudes. In the absence of inertial cavitation, the amplitude of the direct photoacoustic response is below the noise level of the system. Our prior work, using small nanoparticle doped spherical targets, indicated that photoacoustic emission levels are well below signal levels generated by inertial cavitation and the timing of inertial bubble collapse lags the photoacoustic signal by approximately one half of a cycle of the externally applied sound field. This is wholly consistent with the argument that nano-scale vapor cavities induced by particle heating serve as nucleation sites for acoustic cavitation activity. The nanoscale bubbles are made to grow during the rarefaction phase of the ultrasound and collapse inertially during the compression phase, roughly one half cycle later [33]. In the present experiments, the nanoparticles are dispersed in a liquid and the photoacoustic response is not spatially confined, leading to poor photoacoustic generation efficiency over the bandwidth of the detection transducer. However, we see the same sudden onset of strong acoustic emission at a threshold fluence level and attribute this to inertial cavitation. The cavitation probability as a function of laser fluence is given in Fig. 2(b) for ultrasound pressures in the 1.5-3.0 MPa range. Here, 1000 measurements were taken at each laser fluence-ultrasound pressure combination, with a laser repetition rate of 20 Hz.

Referring to Fig. 2(b), the fluence required to initiate cavitation is quite small and seen to reduce significantly as the peak HIFU rarefaction pressure increases from 1.5 MPa to 3.0 MPa. Defining the cavitation threshold fluence as the fluence at which cavitation events are observed 50% of the time, we see a reduction from 4.6 mJ/cm^2 (1.5 MPa) to 2.5 mJ/cm^2 (3.0 MPa). The threshold observed at 1.5 MPa is in reasonable agreement with that measured by Farny *et al.* [32] while those measured at higher pressure are lower than had previously been observed. The shape of the probability curves resembles the typical "S-Curves" predicted in

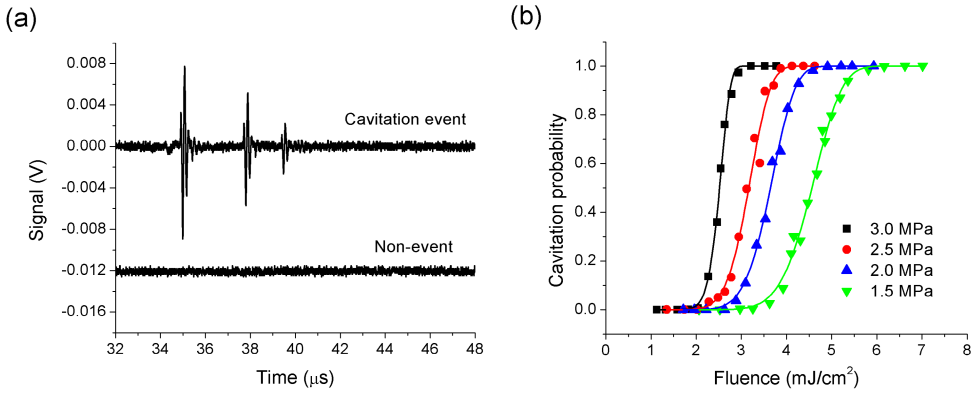

Fig. 2. (a) Acoustic signals from a photoacoustic cavitation event and a non-event around gold nanospheres (2.2×10^8 nanoparticles/ml) at a peak negative HIFU pressure of 1.5 MPa and a laser fluence of 4.8 mJ/cm^2. (b) Cavitation probability as a function of laser fluence around gold nanospheres (2.2×10^8 nanoparticles/ml) at peak negative pressures of 1.5, 2.0, 2.5 and 3.0 MPa. Solid lines are fitted using Eq. (1).

#177949 - $15.00 USD Received 12 Oct 2012; revised 30 Nov 2012; accepted 7 Dec 2012; published 11 Dec 2012

homogeneous nucleation theory [38], and the solid lines on the plot are fitted to a similar functional form of

$$P_n = 1 - \exp\left[-\alpha \exp\left(-\gamma / F\right)\right], \quad (1)$$

where F is the laser fluence and α and γ are used as fitting parameters and are associated with the probability of a nucleation site within the interaction region and the energy barrier to nucleation, respectively. The transition region between the onset of cavitation and cavitation on every laser shot is quite broad and increases with decreasing pressure. At the nanoparticle concentration used, the probability of at least one nanoparticle being in the light-sound interaction region, based on the Poisson distribution, is nearly unity. If all of the particles had identical cavitation thresholds, a sharper transition region governed primarily by spatial and temporal fluctuations in the laser source might be expected. We believe that the broad transition region may be associated with the size distribution of the nanoparticles. The absorption cross section of the nanoparticles is a function of nanoparticle size and thus the temperature rise is also size dependent. A small concentration of larger particles, with a lower cavitation threshold, will have a smaller probability of being in the interaction region at a given time. Referring to the population of nanoparticles that undergo cavitation at a given fluence and pressure as "active nanoparticles," the results indicate that only a fraction of the nanoparticles in suspension are active through the transition region. Note that a cavitation probability of unity does not mean that all of the nanoparticles in the interaction region produce bubbles on every shot, but rather that at least one nanoparticle in this region does. The analysis of the particular form of the probability curves is further complicated by non-uniform pressure-light distribution within the interaction region.

The results of similar experiments performed on nanorods at a concentration of 5.7×10^8 particles/ml are shown in Fig. 3 for ultrasound peak negative pressures of 1.8 MPa (Fig. 3(a)) and 2.5 MPa (Fig. 3(b)). The open circles show the measured probability curve in unmixed nanorod suspension at a laser repetition rate of 20 Hz. The solid circles show measurements made at the laser repetition rate of 1 Hz and with a magnetic mixer added to the suspension to facilitate rapid replenishment of the nanoparticle suspension in the interaction region between measurements. Under both ultrasound pressures, the two curves are similar up to a laser fluence of approximately 2.0 mJ/cm^2. Beyond this point, the probability curve measured in the unmixed suspension becomes erratic and does not reach 100% probability in the fluence range shown, while the mixed suspension shows the same general behavior as the nanospheres. We believe that the divergence in these curves is due to permanent bleaching of the nanorods in

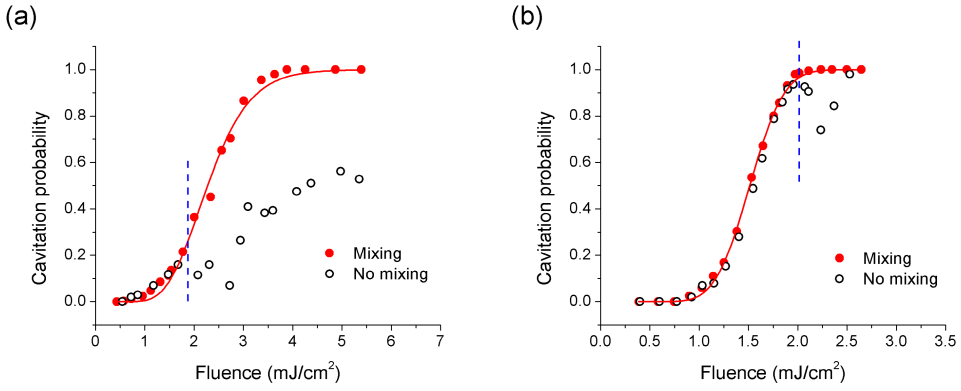

Fig. 3. Cavitation probability around mixed (solid circles) and unmixed (open circles) gold nanorods (5.7×10^8 nanoparticles/ml) as a function of laser fluence at peak negative pressures of (a) 1.8 MPa and (b) 2.5 MPa. Vertical dash lines show the nanorod damage threshold. Solid lines are fitted using Eq. (1).

#177949 - $15.00 USD Received 12 Oct 2012; revised 30 Nov 2012; accepted 7 Dec 2012; published 11 Dec 2012

the interaction region leading to depletion of at least some of the nanorods. The observed damage threshold is lower than the 5 mJ/cm^2 found for 10 nm × 41 nm gold nanorods using transmission measurements [29]. However, this discrepancy may be caused by the different size and aspect ratio of the nanorods. It may also be associated with the measurement approach, where the cavitation measurements may indicate depletion of a small population of nanorods with favorable characteristics (shape and orientation) for cavitation.

The nanorods probability curves for mixed suspensions over the pressure range from 1.8 to 3.0 MPa are shown in Fig. 4(a). The curves show the same general features as the nanospheres, with the notable exception of lower threshold fluences which decrease from 2.3 mJ/cm^2 at a pressure of 1.8 MPa to 1.3 mJ/cm^2 at a pressure of 3.0 MPa. The cavitation thresholds for nanorods and nanospheres are compared in Fig. 4(b). The vertical line shows the maximum ultrasound exposure specified for diagnostic ultrasound equipment, at a mechanical index (MI) of 1.9 [39]. The horizontal line shows the damage threshold measured for the nanorods. At the maximum MI, we find a nanosphere cavitation threshold of approximately 4.0 mJ/cm^2 and a nanorod cavitation threshold of approximately 2.3 mJ/cm^2. The nanorod threshold fluence is lower than any previously reported for any type of nanoparticle in water in the absence of an applied ultrasound field. In terms of the nanorod damage threshold, it is seen that the cavitation threshold near the MI is above the damage threshold. However, it is still possible to achieve cavitation in below the damage threshold as indicated in Fig. 3, albeit with a reduced probability of approximately 18%.

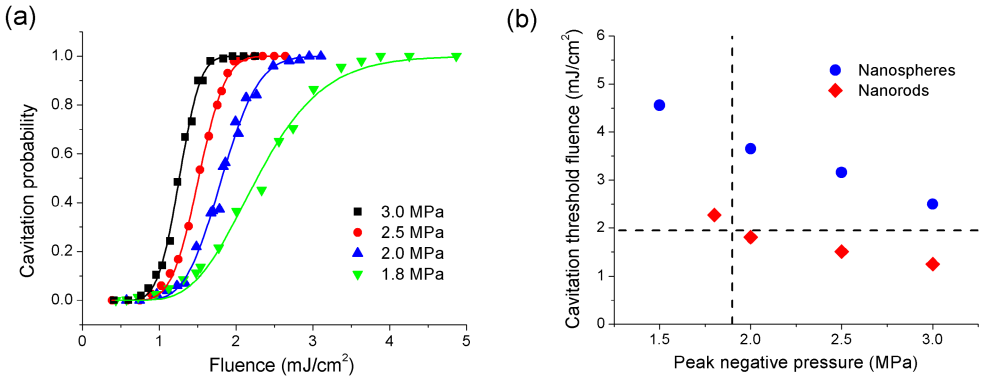

Fig. 4. (a) Cavitation probability as a function of laser fluence around mixed gold nanorods (5.7 × 10^8 nanoparticles/ml) at peak negative pressures of 1.8, 2.0, 2.5 and 3.0 MPa. Solid lines are fitted using Eq. (1). (b) Cavitation threshold fluences around gold nanospheres (2.2 × 10^8 nanoparticles/ml) and gold nanorods (5.7 × 10^8 nanoparticles/ml) at different peak negative pressures. The vertical dashed line is the mechanical index limit for diagnostic ultrasound at 1.0 MHz. The horizontal dashed line is the nanorod damage threshold.

Typical acoustic signals generated during nanorod cavitation events are shown in Fig. 5(a) for laser fluences of 1.3 mJ/cm^2, 4.1 mJ/cm^2, and 13.0 mJ/cm^2 and for a peak negative pressure of 1.8 MPa. The peak-to-peak amplitude of the acoustic signals as a function of laser fluence is shown in Fig. 5(b). As the laser fluence is increased, the amplitude of the acoustic emission increases. This effect is most likely due to an increase in the number of nanoparticles within the interaction region that produce bubbles. In addition, the shape of the acoustic signal broadens and at higher fluence acoustic arrivals associated with bubble rebound events are observed. This is consistent with an increase in the volume of liquid within which the pressure/fluence combination is sufficient to produce cavitation events. We also find that the amplitudes appear to saturate in the 11-14 mJ/cm^2 range. While the reason for this is not well understood, it may be associated with a saturation of the number of nucleation sites (nanorods) within the interaction volume. The ultrasound pressure decreases rapidly outside of the focal region essentially limiting the volume of liquid within which the critical

#177949 - $15.00 USD Received 12 Oct 2012; revised 30 Nov 2012; accepted 7 Dec 2012; published 11 Dec 2012

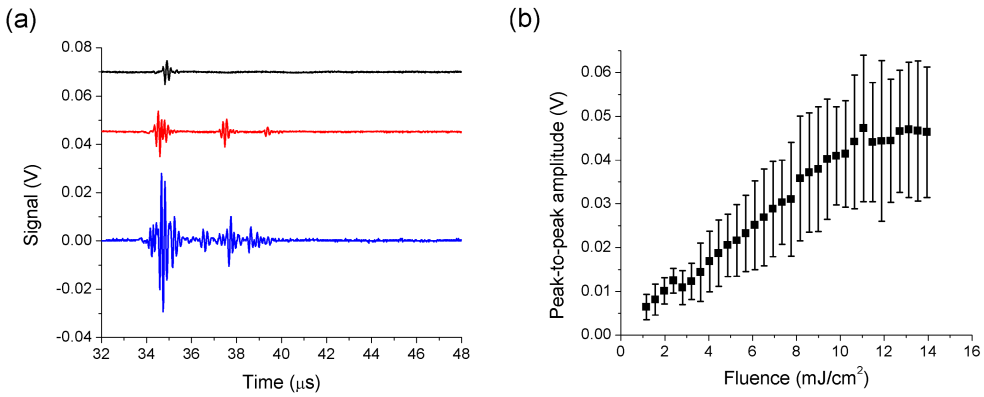

Fig. 5. (a) Acoustic signals emitted from photoacoustic cavitation events around mixed gold nanorods (5.7×10^8 nanoparticles/ml) at a peak negative pressure of 1.8 MPa and fluences of 1.3 mJ/cm^2 (black line), 4.1 mJ/cm^2 (red line), and 13.0 mJ/cm^2 (blue line). (b) Peak-to-peak amplitude of the acoustic signals from photoacoustic cavitation events around gold nanorods (5.7×10^8 nanoparticles/ml) as a function of laser fluence at a peak negative pressure of 1.8 MPa. Symbols and error bars are the mean values and standard deviations of the amplitude.

conditions (fluence and pressure) are satisfied. We note that even at the smallest laser fluence, the inertial collapse of bubbles produces an exceptionally strong photoacoustic signal which can potentially be used to monitor a therapeutic process.

Cavitation probability as a function of nanoparticle concentration was also explored. The results for nanospheres at several different fluences and peak negative pressures of 2.0 and 3.0 MPa are shown in Figs. 6(a) and 6(b) respectively. As the concentration is reduced, there is a lower probability of a nanoparticle in the interaction region. The probability that at least one nanoparticle is in the interaction region is given by

$$P = 1 - \exp(\rho V), \tag{2}$$

where ρ is the nanoparticle concentration and V is the effective volume of the interaction region. The curves in Fig. 6 have been fitted with this expression using V as a free parameter. The effective volume was found to increase as ultrasound pressure and laser fluence increase. Furthermore, the effective volume found based on the curve fits is 20-100 times smaller than the estimated interaction volume, based on the full-width at half maximum (FWHM) of the optical and ultrasound beams, of approximately 1.0 mm^3. This provides further evidence that

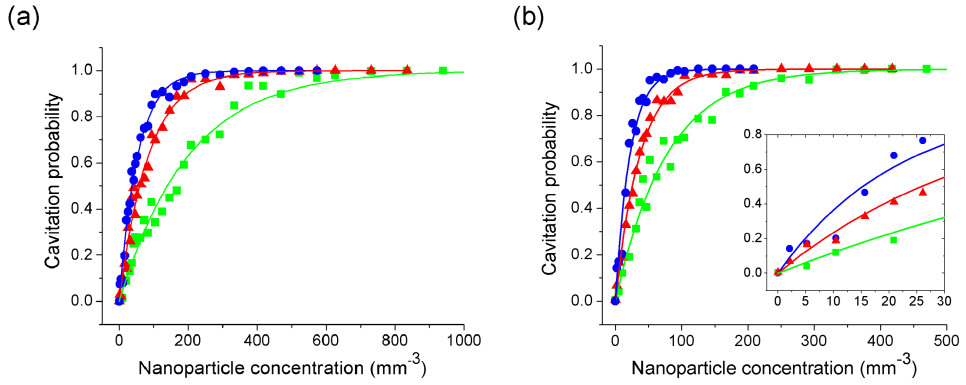

Fig. 6. Cavitation probability as a function of nanoparticle concentration around gold nanospheres at peak negative pressures of (a) 2.0 MPa and (b) 3.0 MPa and fluences of (●) 7.6 mJ/cm^2, (▲) 6.5 mJ/cm^2 and (■) 5.4 mJ/cm^2. Solid lines are fitted using Eq. (2). Inset of (b) is a zoom-in of the probability curves at 3.0 MPa.

#177949 - $15.00 USD Received 12 Oct 2012; revised 30 Nov 2012; accepted 7 Dec 2012; published 11 Dec 2012

there is a relatively wide distribution of cavitation thresholds within the nanoparticle population; potentially due to size dispersion. Returning to the concept of active nanoparticles at a given laser fluence-ultrasound pressure combination, this result indicates that only a fraction (~1/20–1/100) are active under these conditions. As either the fluence or pressure is increased, the population of active nanoparticles also increases. The inset in Fig. 6(b) shows a zoomed in region of the probability curve. It is possible to excite, and detect, cavitation events in extremely dilute nanoparticle concentrations. Nanosphere concentrations as small as 10 nanoparticles/mm^3 produce a detectable change in the cavitation probability.

Figure 7 shows the cavitation probability as a function of concentration for nanorods. Here, a single optical fluence is selected which is just below the nanorod damage threshold, and measurements are taken under a relatively high peak negative pressure of 3.0 MPa. The curve shows a marked difference from the nanosphere curve in that the number of nanoparticles required for a given cavitation probability is about 3 orders of magnitude higher. This is in part due to the fact that the fluence used is closer to the threshold fluence in the nanorod case, thus potentially leading to a lower population of active particles, but it is also associated with the orientation dependence of the optical absorption. Random orientation of the particles with respect to the incident linearly polarized light leads to a broad distribution in optical absorption efficiency and threshold fluence for cavitation.

We now consider the potential for using photoacoustic cavitation to produce targeted bubble formation at depth in soft biological tissue. Here we limit the discussion to ultrasound pressures not exceeding the maximum MI for tissue. However, operation above the MI limit can potentially be used to create nanoparticle targeted bubbles for enhanced local heating in HIFU therapy. The fluence threshold for nanospheres and nanorods at the MI limit are 4.0 mJ/cm^2 and 2.3 mJ/cm^2, respectively. The maximum permissible exposure (MPE) at 532 nm is 20.0 mJ/cm^2 and that at 724 nm is 22.3 mJ/cm^2 [40]. Taking breast tissue as an example [41], the effective attenuation is approximately 7.8 cm^{-1} at 532 nm and 1.2 cm^{-1} at 724 nm. This yields a maximum depth at which photoacoustic cavitation can be achieved of 0.2 cm in the case of nanospheres and 1.9 cm in the case of nanorods. This can potentially be increased through optimization of nanoparticle type and shape. Promising candidates in this regard include gold nanoshells and gold coated nanorods [22,26–28], both of which exhibit lower optical cavitation thresholds than nanorods in the absence of an ultrasound field.

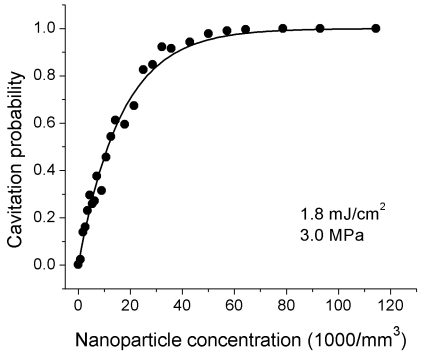

Fig. 7. Cavitation probability as a function of nanoparticle concentration around gold nanorods at a peak negative pressure of 3.0 MPa and a fluence of 1.8 mJ/cm^2. Solid line is fitted using Eq. (2).

4. Conclusions

The nanoparticle-mediated interaction of light and sound can potentially be used to produce cavitation within biological tissue at laser fluences that are significantly lower than can be achieved using light alone. A detailed *ex vivo* experimental study has been performed on

#177949 - $15.00 USD Received 12 Oct 2012; revised 30 Nov 2012; accepted 7 Dec 2012; published 11 Dec 2012

photoacoustic cavitation generated by simultaneously exposing gold nanorods and nanospheres to laser light and focused ultrasound. The results demonstrate the significant impact of the applied ultrasound field on the nucleation and amplification of the cavitation process. For both nanorods and nanospheres in diagnostically relevant acoustic fields, the measured cavitation threshold fluence is well below the MPE for tissue. The likelihood that a given nanoparticle will nucleate a cavitation event increases with both fluence and peak negative acoustic pressure amplitude, and is not the same for all particles. This latter effect can be attributed to size dispersion in the case of nanospheres, with the larger particles absorbing more optical energy and thus having lower threshold fluences. In the case of nanorods, both size dispersion and nanoparticle orientation may lead to threshold fluence variations. Results indicate that even with relatively low nanoparticle concentrations, cavitation bubbles can be produced around these nanoparticles and that the collapse of said bubbles results in a local mechanical disruption and associated strong acoustic emission. These effects can be achieved at well below the MPE for tissue and MI limit for diagnostic ultrasound, making the approach attractive for both inducing and monitoring nanoparticle-mediated tissue therapy.

#177949 - $15.00 USD Received 12 Oct 2012; revised 30 Nov 2012; accepted 7 Dec 2012; published 11 Dec 2012